JOURNAL OF MATERIALS SCIENCE **35** (2000) 5029–5045

Optimisation of second order non linear optical properties in two dimensional SHG chromophores by using modern electron crystallography

I. G. VOIGT-MARTIN
Institut für Physikalische Chemie der Universität Mainz, Jakob Welder Weg 11, D55099 Mainz, Germany
E-mail: voigtmar@mail.uni-mainz.de

It is shown how new methods of electron crystal structure analysis can be used to probe the physico chemical parameters of two dimensional second harmonic generation (SHG) chromophores at a molecular level and how these can be influenced in order to enhance specific properties of the macroscopic material.

1. Introduction: Basic concepts in non-linear optics

Organic materials have the enormous advantage that their molecules can be tailored to produce specific physical effects and the resulting materials can easily be processed in the desired geometry. However, molecular properties can only be fully utilised if molecules are suitably dispersed in a matrix or if their orientation in the resulting crystals is such that their molecular properties are enhanced. In order to achieve this, special measures are frequently required. A number of particularly interesting properties can be achieved if the crystals are non-centro symmetric. Examples are:

1. Second harmonic generation	FREQUENCY DOUBLING
2. Ferroelectricity	POLARISATION DIRECTION FIELD DEPENDENT
3. Triboluminescence	LIGHT EMISSION DUE TO MECHANICAL STRESS
4. Piezoelectricity	CHARGE SEPARATION DUE TO COMPRESSION
5. Pyroelectricity	CHARGE MIGRATION UNDER THERMAL STRESS

In this work we hope to demonstrate that a fundamental understanding of the relationship between the structure of organic molecular crystals and their macroscopic second order non-linear optical (NLO) properties can be used to improve the observed effect considerably. The further aim is to find a more specifically directed route toward the synthesis of molecules with the required molecular architecture.

Such an approach requires close collaboration between specialists in organic chemistry, physical chemistry and physics as well as in electron microscopy and can be described by the term "crystal engineering" [1].

The effect which is observed in second order NLO is that of frequency doubling, or second harmonic generation (SHG). In our examples, an incoming beam of infrared light ($\chi = 1047$ nm) emerges as green light ($\chi = 523.5$ nm). Practical applications are found in opto-electronic devices which process information efficiently and are therefore candidates for future communication systems. Organic materials have SHG efficiencies which are much larger than those of classical inorganic materials like lithium niobate or potassium dihydrogen phosphate, a positive effect which is unfortunately coupled with poorer mechanical properties.

The observed physical property involved is the optical susceptibility χ which is related to the polarisation P by the following expression:

$$P = \varepsilon_0\left[\chi_{IJ}^{(1)}E + \chi_{IJK}^{(2)}E^2 + \chi_{IJKL}^{(3)}E^{3\ldots}\ldots\right] \quad (1)$$

where P is the polarisation, E the electric field, χ_{IJ} the linear susceptibility, χ_{IJK} the second order susceptibility, χ_{IJKL} the third order susceptibility. The macroscopic term relevant for SHG, namely χ_{IJK}, can be non-zero only if the crystal is non-centrosymmetric.

In addition to the macroscopic crystallographic aspects, there are microscopic molecular criteria which need to be considered. For organic compounds the molecular dipole moment μ induced by an electric field E is given by:

$$\mu_i = \mu_i^0 + \alpha_{ij}E + \beta_{ijk}E^2 + \gamma_{ijkl}E^3\ldots \quad (2)$$

where μ_i^0 is the intrinsic molecular dipole moment and i, j, k, l are related to the molecular co-ordinates. The molecular polarisability α and the second and third order hyperpolarisabilities β, γ are given in the molecular co-ordinate system. The molecular parameter relevant for SHG is β_{ijk}, the hyperpolarisability. Its value

depends on the conformation of the molecule i.e. the precise positions of its constituent atoms.

Second order susceptibility in crystals is possible only if these are non- centrosymmetric. In order to ensure that a molecule crystallises in the required manner, the molecular architecture is often specifically designed by using physico- chemical concepts such as the following [1].

1. Molecular chirality
2. Hydrogen bonding to produce chiral arrays
3. Reduction of ground state dipole to prevent anti-parallel arrangement
4. Orientation by crystal growth in an electric field
5. Orientation in Langmuir-Blodgett films
6. Polymers which form self-assembled films
7. Organic molecules which form liquid crystals

The relationship between microscopic and macroscopic parameters is given by:

$$\chi_{IJK}(-2\omega;\omega_1,\omega_2) = \frac{N}{V}\Bigg[f_I(\omega) f_J(\omega) f_K(\omega) \times \sum\sum \cos\theta_{Ii} \cos\theta_{Jj} \cos\theta_{Kk} \beta_{ijk}(-2\omega,\omega_1,\omega_2)\Bigg] \quad (3)$$

where V is the unit cell volume, N is the number of molecules per unit cell, $f_i(\omega)$ are local field factors at frequency ω for the I-direction in the crystal and the θ_{Ii} are the rotation angles relating microscopic molecular and macroscopic crystal axes. The local field factors $f_I(\omega)$ depend on the linear polarisability term α_{Ii}, which is related to the refractive indices of the crystal. The macroscopic susceptibility coefficients d_{IJK} which are actually measured in an experiment are directly related to χ_{IJK} and to the direction of the incoming and outgoing beams with respect to the crystal axes. They depend on the crystal symmetry.

The macroscopic properties thus depend on the atomic positions in the unit cell and on its symmetry. This information can only be obtained by structure analysis and refinement.

The classical way of determining and refining structure is by X-Ray diffraction. Here Zyss and his collaborators have made major contributions in relating molecular properties to crystal structure [2]. However there are many molecules which do not crystallise easily or which form crystal platelets which are only about 10 nm thick with lateral dimensions of a few tens of nanometres. For such materials electron crystallography is the only solution.

In recent years there have been enormous advances in electron crystallography, which can be summarised as follows:

1. Traditional direct methods (triplets, Sayre equation, Tangent formula) [3].
2. Maximum entropy and log likelihood [4–13, 18–21].
3. Calculation of exit wave (Bloch Formalism) [14]
4. Simulation of electron diffraction patterns and images (quantum mechanical calculations, packing energy calculations) [8–13, 18–21].

Our approach to electron crystallography, which involves quantum mechanical and molecular packing calculations combined with the Maximum Entropy approach, offers the advantage of giving deeper insight into the molecular mechanisms which give rise to the observed physical properties, as will become apparent in the following.

2. Outline of experimental procedure

The basic consideration is therefore to relate the following:

Molecular architecture

↓

Characterisation of molecular parameters

↓

Structure and relation of molecular properties to crystal axes

↓

Physical properties

Our experimental procedure can be summarised in the following 14 steps:

1. A molecule with a suitable chemical architecture is synthesised according to the principles outlined above.
2. It is established whether the molecule has a NLO effect in solution by EFISH (Electric Field Induced Second Harmonic Generation) and Hyper Rayleigh Scattering methods and μ, α, β are measured [13]
3. The conformation of the molecule in the gas phase is calculated by semi-empirical methods using MOPAC [15], or *ab initio* quantum mechanical calculations with GAUSSIAN OR TURBOMOL [16]
4. Molecules are oriented in the crystal to produce non-centrosymmetry by using methods outlined above.
5. Crystals are screened to establish NLO effect [17].
6. Electron diffraction patterns are obtained in at least 8 different projections [8–13, 18–21]
7. Electron diffraction intensities are quantified [11, 12, 22, 23]
8. Routine check of d-values with X-ray powder diffraction is performed [8–13, 18–21]
9. Electron diffraction patterns are simulated and packing energy calculations performed [8–13, 18-21]
10. High resolution imaging and image restoration is carried out [8, 12]
11. Images are simulated [8, 12]
12. Effect of dynamical scattering is considered [8–13, 18–21]
13. *Ab initio* structure is determined using maximum entropy approach [8–13, 18–21]
14. Molecular α, μ, β are related to crystal co-ordinates by a suitable co-ordinate transformation and macroscopic optical susceptibilities calculated [8–13, 18–21].

3. Experimental methods and results

3.1. Choice of suitable chemical architecture

Generally linear molecules are chosen which give rise to a one-dimensional charge transfer along the molecular axis. In the case of such such one-dimensional SHG-chromophores, the molecular first hyperpolarizability tensor, β_{ijk}, has a dominant vectorial contribution

$$(\beta)_i = \sum_j \beta_{ijj}$$

where the i-axis is parallel to the charge transfer direction and β_{iii} is the dominant tensor component. Linear molecules often crystallise centro symmetrically because the major dipole components lie along the molecular axis and tend to oppose each other in the crystal. In order to avoid this, a series of two dimensional molecules were synthesised.

In this paper we describe the molecular and crystallographic parameters relevant for SHG-efficiency of two-dimensional SHG-chromophores. The structural data were used to calculate the angular parameters of the molecular orientations in the cell and to relate the crystalline non-linear tensor coefficients b_{IJK} to the components of the molecular β-tensor. An estimation of the refractive indices of the crystals along the crystal axes and the corresponding local-field factors, relating the b_{IJK}-coefficients to the experimentally measurable macroscopic d_{IJK}-coefficients, was performed based on the calculated molecular linear polarizability tensor α, reduced to the crystal axes frame.

On the basis of these calculations predictions can be made regarding the suitability of a specific molecule for SHG applications.

The molecules chosen for this two dimensional charge transfer are shown schematically below. They were synthesised in the group of A.Tenkovtsev. In the diagram below we have included the space group which was determined by electron diffraction in bold print:

190. 2,6-bis(4-hydroxy-benzylidene)-cyclohexanone (**BHBC**); **Pna2$_1$**

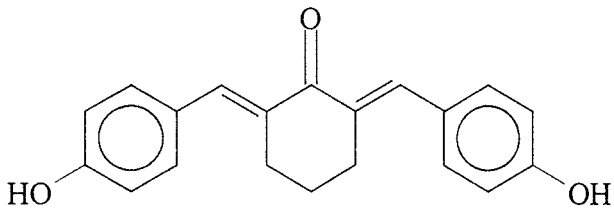

191. 2,6-bis(4-dimethylamino-benzylidene)-cyclohexanone (**DMABC**); **CmC2$_1$**

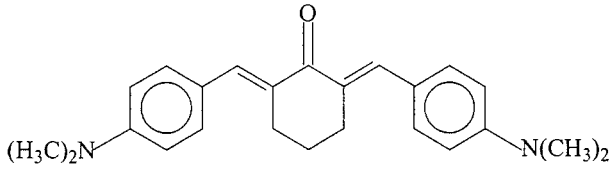

192. 2,6-bis(4-dimethylamino-benzylidene)-acetone (**DMABA**); **P2$_1$**

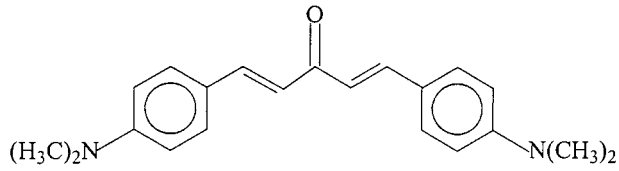

197. **BMHBC/POL**; $n = 6$; **P2$_1$11**

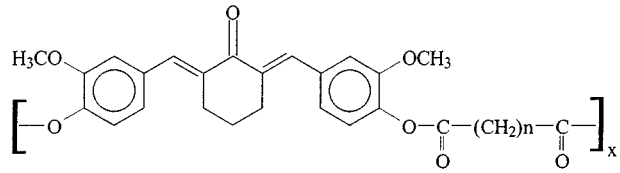

199. 2,6-bis(3-methoxy-4-hydroxy-benzylidene)-cyclohexanone (**BMHBC**); **P2$_1$/c**

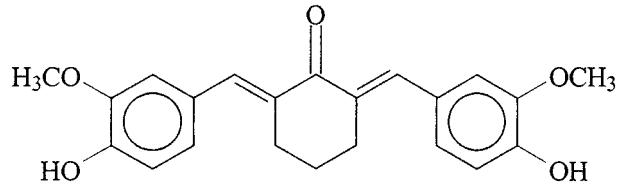

3.2. Screening molecules for NLO effect

3.2.1. Hyper Rayleigh Scattering (HRS)

The Hyper Rayleigh Scattering technique [24, 25] is a method of determining the molecular second order hyperpolarisability. By collecting the frequency doubled light scattered perpendicular to the propagation direction of an intense laser beam in an isotropic liquid, one obtains information about the second order polarisability of the solute. If the experiment is performed under different polarisation conditions of the fundamental laser and the collected light, it is possible to determine five independent terms containing products of β components. We have described details about these calculations on other molecules in the specialised literature [13]. If only one β component is significant (as is the case in many linear molecules with delocalised π-system) the molecular fixed frame may be chosen such that the tensor components which finally emerge after some calculation are β_{xxx}, β_{yyy} or β_{zzz}. These components are then easy to relate to those calculated by MOPAC in semi-empirical quantum chemical calculations.

3.2.2. Electric field induced second harmonic generation (EFISH)

The EFISH technique [26] utilises a static electric field E_0 to induce an effective second order susceptibility

$$\chi^{(2)}(-2\omega;\omega,\omega;E^0) = 3\chi^{(3)}(-2\omega;\omega,\omega,0)E^0$$

in a liquid solution.

The evaluation of concentration dependent EFISH measurements yields partial molar third order polarisabilities. Finally with the ground state dipole obtained from permittivity measurements, it is possible to evaluate the vector parts of the second order polarisability. Thus the value of β which is obtained is its projection on μ. We have reported detailed results on 4-Dimethylamino-3-cyanobiphenyl elsewhere [13, 21].

3.3. Generation of a molecular model and determination of gas phase polarisability α, dipole moment μ and hyperpolarisability β

From quantum mechanical calculations we can only obtain the gas phase conformation of the molecule. However, it has been shown that crystallisation generally affects only the torsion angles of the molecule [27, 28], therefore the gas phase conformation is often sufficiently accurate to use as a starting conformation for the packing energy calculations which have to be performed subsequently.

While the semi-empirical AM1 and PM3 values calculated by MOPAC are normally sufficiently accurate to initialise the crystallography programs, in the case of the 2-D molecules discussed here it was found that the conformation differences between *ab initio* and semi empirical calculations were by no means negligible, as will be seen in the following.

Second order polarizabilities are frequently defined using differing conventions, so it should be noted that the semi-empirical calculations use the finite field technique [29]. These methods have been parametrized for gas phase properties such as ground state geometries, dipoles μ and heats of formation, but not for the second order polarizability β. Generally the second order polarizability values obtained by these methods are intermediate between those obtained by self-consistent field (SCF) and second order perturbation (MP2) calculations.

When comparing the values for β with the results of the spectroscopic measurements, the finite field method incorporated in MOPAC gives values for the static second order polarizabilty $\beta(0;0,0)$. The optical values $\beta(-2\omega;\omega,\omega)$ obtained from the experiments are enhanced with respect to the static ones by dispersion and by the influence of the reaction field in solution [30–32]. In general the calculated values are therefore expected to be significantly lower than the ones obtained experimentally. In order to obtain frequency dependent values, it is necessary to resort to *ab initio* quantum mechanical calculations using programs such as TURBOMOL or GAUSSIAN.

In our work, therefore, the *ab initio* density functional theory (DFT) approach [33] implemented into the TURBOMOLE program package [34] was also used to calculate the equilibrium gas-phase conformation of the molecules (the details concerning basis sets used for the DFT-calculations of these molecules are described in [10–12]). In this way it is possible to correct for inaccuracies of a semi-empirical description of the conformation-determining balance between the π-conjugation and steric repulsion factors.

Taking into account frequency-dependence of the molecular α-tensor and, hence, local-field factor values, f_I, we obtain [19]:

$$\frac{(n_I^2-1)}{(n_I^2+2)} = \left(\frac{4}{3}\right)\pi\left(\frac{N}{V}\right)\alpha_{II} \text{ (Lorenz-Lorentz relations)}$$

$$\Rightarrow f_I = \frac{(n_I^2+2)}{3} = \frac{1}{\left[1-\left(\frac{4}{3}\right)\pi\left(\frac{N}{V}\right)\alpha_{II}\right]}$$

where α_{II} are the diagonal components of the α-tensor of the unit cell per molecule.

The *ab initio* α-tensor calculations were performed with the 6-31G basis set augmented with polarization p- and d-functions at hydrogen and non-hydrogen atoms respectively, and with diffuse s-functions at all atoms, hereafter referred to as 6-31G(+sp, +sd) basis set [11], which is specially optimised for molecular polarizability calculations [35].

3.4. Screening crystals for NLO effect

Images showing the effect of frequency doubling (in this case infrared $\rightarrow$ green) can be obtained using an SHG-microscope [17]. This experiment gives a purely qualitative indication as to whether a sample is SHG active or not. The core of the set-up is an Olympus measuring microscope, which is adapted for imaging the SHG signal as well as for dark field polarisation and fluorescence-microscopy. The fundamental beam of a Q-switched Nd : YLF laser ($\lambda = 1047$ nm) provides light pulses in the range of 100 mJ (15 ns, at a repetition rate of 3000 Hz).The incident laser beam (TEM_{00} beam diameter 0.9 mm, polarisation 100 : 1) is focussed via a beam-steering mirror onto the crystal in diascopic geometry. The resulting fundamental intensity in the plane of the crystal is of the order of 10^{12} W/m^2. In order to protect the lens system and the sample against the high power laser pulses an infrared filter (Schott BG 40, transmission at 1047 nm $= 10^{-4}$) was placed in front of the objective lens. An additional band pass filter guarantees that only the second harmonic light reaches the detector. We have demonstrated the effect with colour micrographs in the specialised literature [17].

3.5. Electron diffraction

The experimental electron diffraction patterns from the organic thin crystals must be compared with the calculated diffraction patterns obtained from a model of the molecules in the unit cell belonging to the appropriate space group. In order to determine the space group from the extinctions, it is necessary to obtain a large number of projections experimentally [8–13, 18–21]. This can be very demanding experimentally for unknown structures and beam sensitive samples. In this way it is also possible to establish the cell constants and, by applying the required trigonometric relationships, the cell angles.

It has been shown in many publications that intensities are affected and extinctions may be masked by

a large number of factors such as dynamic scattering [36], crystal bend or buckling [3] and beam damage [37].

Single crystal electron diffraction data at 100 kV were obtained with a Philips 420 scanning transmission electron microscope, using a rotation-tilt holder in order to obtain diffraction patterns from suitable crystallographic zones and a low dose unit to reduce beam damage. The maximum tilt angle is 60°, so that for flat crystals there is a cone of 30° in any specific crystal which contains zones inaccessible to electron diffraction. The instrument was carefully aligned and the sample tilted about specific axes as described previously [8–13, 18–21]. The data were registered on film emulsion and their quantitative values determined using ELD [38].

Other sets of single crystal diffraction data were obtained with a Philips CM30 UT electron microscope with a field emission gun operated at 300 kV [11, 12]. In this case, the tilting axes were not specified and arbitrary diffraction patterns were obtained from successive zones. The patterns were recorded using a 1024×1024 pixel Gatan CCD camera with a dynamic range of 14 bits. The illuminated area on the crystal was so small (typically around 30 nm) that only one crystal contributed to the pattern. With the field emission gun it is possible to produce such spots with an almost parallel bundle. The exposure times ranged from 100 to 600 ms. These values were short enough to avoid problems of damaging the sample too much. X-ray powder diffraction data were also used to increase the accuracy of the lattice spacings obtained from the electron diffractograms and to obtain information regarding dynamical or secondary scattering . If specific higher order peaks appear in electron diffraction but are absent in the X-ray diffractograms this can be an indication for dynamic scattering. For X-ray powder diffraction investigations, a Siemens D-500 diffractometer in the $\Theta/2\Theta$ reflection mode (Cu K_α-radiation with $\lambda = 0.1542$ nm) was used.

3.6. Quantifying electron diffraction patterns

3.6.1. 100 kV data

The 100 kV electron diffraction data were scanned with a Nikon LS 4500 AF scanner at a resolution of 1600 d.p.i. and transferred to a PC for quantifying using the ELD software [38]. Recently there have been considerable improvements in this program so that more accurate data can be obtained. It is essential to ensure that ELD is evaluating the intensities in saturation correctly by studying exposure series. It is also essential to calibrate the film emulsion. This can now be done quite quickly with the appropriate software [38, 39]. It is shown here that the accuracy of intensity data can be considerably improved by the use of an on-line slow scan CCD camera with a better resolution and a larger dynamic range.

The quantitative values are first compared with those expected kinematically from the initial model. Each zone is inspected individually for signs of secondary or dynamical scattering. The quality of the data as well as the accuracy of the model are assessed by the *R*-value, defined as in X-ray scattering by:

$$R = \frac{\sum_{hkl} \| F_0 | - | F_c \|}{\sum | F_0 |}$$

The *R*-values are calculated using SHELX 93 [40] but inserting electron instead of X-ray scattering factors.

3.6.2. 300 kV data

The 300 kV data obtained from the CCD camera were evaluated directly with MSLS [11, 12]. MSLS is able to perform a crystal structure refinement based on electron diffraction data and does a full dynamic calculation with the Multi-Slice algorithm [23]. This gives more accurate results than can be obtained with kinematical programs. The parameters to be refined are, besides the ones which are usual in single-crystal X-ray diffraction (i.e., atomic coordinates, Debye Waller factors), crystal properties like crystal tilt, absorption and crystal thickness. These extra parameters are a bonus for using a full dynamical calculation. An additional advantage of accounting for dynamical scattering is the fact that the relative contribution of an atom is not only determined by its atomic weight (as with X-rays), but also by the thickness of the crystal. By selecting a good set of data sets with different thicknesses, it is possible to have all atomic types contributing with the same weight to the resulting set of reflections.

3.7. Simulation of diffraction patterns

On the basis of the electron diffraction patterns combined, if possible, with powder X-ray data, a first model is built up in the Crystal Packer of CERIUS, a program which calculates the packing energy of the crystal. This is a force field approach with the limitations which we have pointed out previously [8–13, 18–21]. For the molecules studied here, the optimal conformation of the central cyclohexanone part (Fig. 1) in a gas phase can differ from that in the crystal. This difference cannot be removed by the Crystal Packer because it does not optimise subrotations within cyclic molecular fragments.

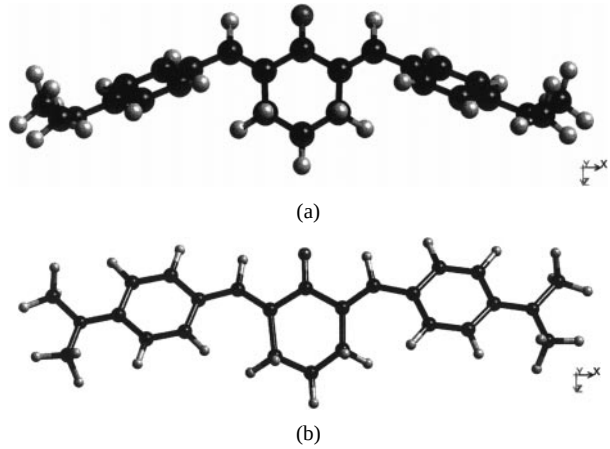

(a)

(b)

Figure 1 DMABC conformation calculated by (a) semi-empirical PM3 and (b) *ab initio* methods.

The simulations of the electron diffraction patterns from all zones and of the X-ray powder pattern were performed by placing the molecule into the unit cell with cell parameters and space group obtained from the electron diffraction analysis. Initially the conformation obtained from quantum-chemical calculations is used. Usually, semi-empirical PM-3 calculations reproduce bond geometry (bond lengths and bond angles) quite reasonably. The packing energy calculations were performed using CERIUS 2.0. On the basis of the known density and symmetry obtained from the electron diffraction data, it is usually possible to find an initial model quite quickly. To account for crystal field effects, slight adjustments to torsion angles are frequently required. Finally reasonable negative packing energies must be achieved. In this series of molecules, *ab initio* calculations lead to a modified molecular gas-phase geometry. This geometry was considerably more favourable regarding molecular packing in the unit cell and was therefore used for the initial model.

After slight adjustments to optimise the packing energy, the model crystal structure was obtained, giving details about the new molecular conformation and arrangement in the unit cell. The first hyperpolarizability tensor components for the asymmetric unit of the unit cell were then calculated for the crystal state molecular conformation and related to the crystal axes.

3.8. The maximum entropy method of solving crystal structures

The problem of solving structures of this complexity from electron diffraction data is in strong contrast to solving problems of a similar type using X-ray diffraction data from a good crystalline sample. In the latter case, the completeness of the data to around 0.11 nm resolution and the lack of systematic errors in the intensities make the problem quite routinely solvable, whereas for electrons the reverse is true, and traditional crystallographic techniques will not, in general, work. The maximum entropy (ME) formalism coupled with likelihood evaluation has shown, however, to be a powerful tool in this case. The method has been described in detail in an electron crystallographic environment in previous papers [8–13, 18–21]. The technique is based on the idea of building phasing trees by taking strong diffraction intensities and giving them trial phases. Experimental designs based on coding theory [41] are used to assign these trial phase values. Each set of intensities and their associated phases are subjected to constrained entropy maximisation in which the constraints are the intensities, phases plus other available information e.g. envelopes, non-crystallograhic symmetry etc. Many phase sets are explored at a given level. The process of entropy maximisation predicts new phases and amplitudes that were not used as constraints. Rice type likelihood functions (LLGs) are used which measure how well the reflections that were not subjected to entropy maximisation are predicted when compared to the experimental observations. Phase sets which have high associated LLGs are more likely to be correct than those with low values.

The method is stable irrespective of data resolution, and completeness and is robust with respect to both random and systematic errors, which can in part be modeled in the calculations. The MICE computer program [42] is a practical implementation of the formalism in a crystallographic environment, and was always used in our work.

3.9. Routine check of *d*-values using X-ray powder data

Standard X-Ray powder diffraction patterns were always obtained to refine the *d*-values obtained from electron diffraction. A Siemens D 500 diffractometer (Cu K_α, $\lambda = 0.1542$ nm) in $\theta/2\theta$ X-Ray reflectivity mode was used [8–13, 18–21]. We have tried to use Rietveld methods, but were successful only in refining *d*-values but not atomic positions. This is because frequently we have independent molecules each consisting of several tens of atoms in general positions in space groups of low symmetry. It seems possible that Rietveld methods might be used successfully to refine known organic structures of this complexity, but that would not be addressing the problem discussed in this article.

4. Results

4.1. DMABC

4.1.1. Quantum-chemical calculations of the molecular gas phase conformation

The lowest energy gas phase conformations of the DMABC molecule calculated by the PM-3 and DFT-*ab initio* methods are shown in Fig. 1a and b, respectively.

As is shown in Fig. 1a, the PM-3 method predicts a curved equilibrium gas phase conformation. This seems unlikely for the crystal state because the crystal cell parameters imply an extended DMABC conformation and it was impossible to pack the MOPAC semi-empirically calculated molecule into the experimental determined unit cell. Therefore, when *ab initio* quantum mechanical calculations indicated an extended chain conformation (Fig 1b) and moreover, four of these extended chains could be easily packed into the unit cell with a very low packing energy, the correct density and the correct symmetry, it was concluded that this conformation was probably correct.

4.1.2. Optical measurements

Optical Measurements on DMABC using the method described previously [17] gave a very high intensity of second harmonic generation (SHG) efficiency.

4.1.3. Determination of space group and cell parameters

On the basis of the observed intensity distributions and extinctions (Fig. 2), the space group was determined to be $Cmc2_1$.

The cell parameters were $a = 2.26$ nm, $b = 0.963$ nm, $c = 0.973$ nm.

From these values of cell parameters it is obvious that the asymmetric unit of the unit cell contains four DMABC molecules in order to give a reasonable density. This means that molecules should occupy special positions within the $Cmc2_1$ unit cell (the asymmetric unit of the unit cell is half a DMABC molecule), with

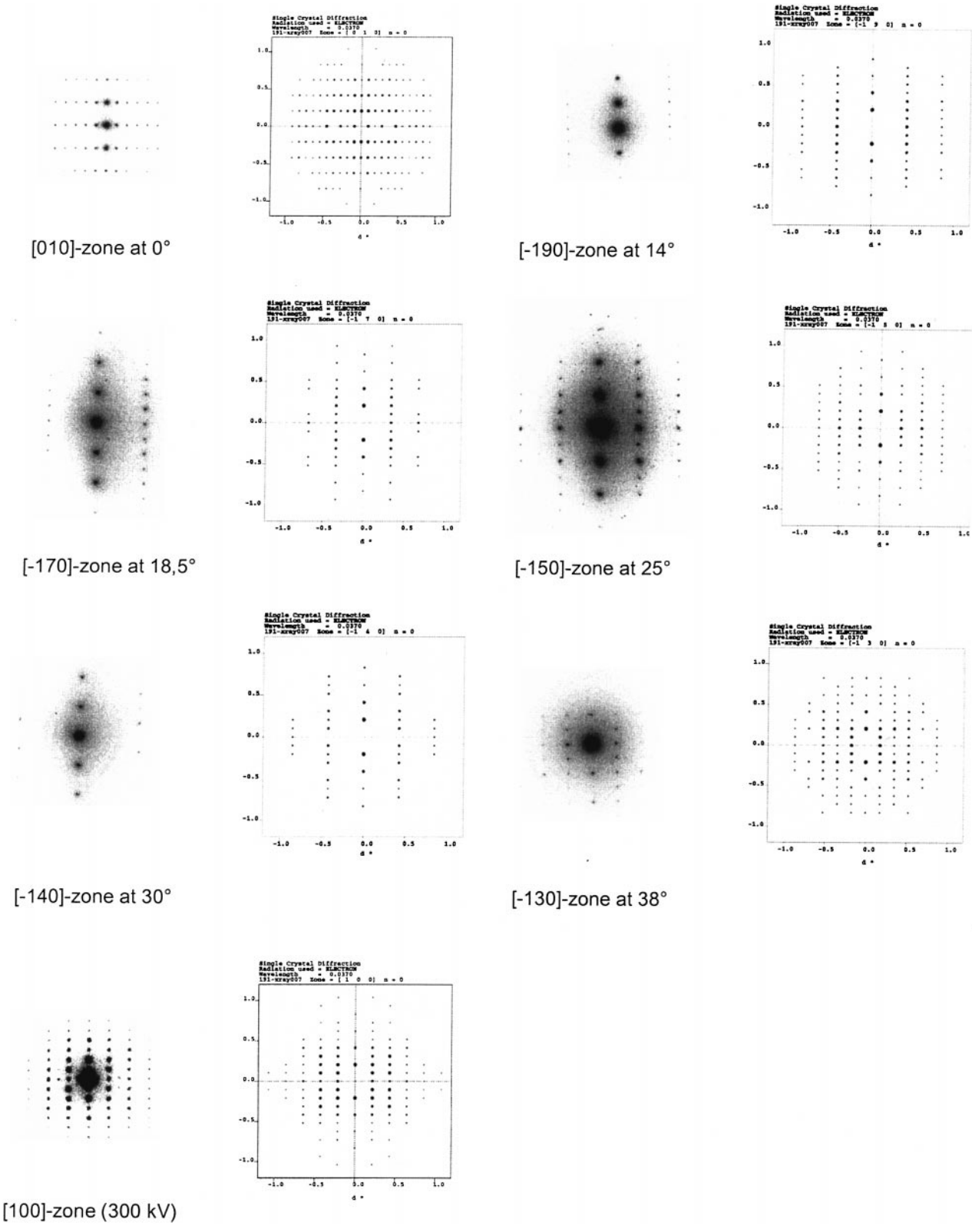

Figure 2 Electron diffraction patterns from DMABC showing different projections (LHS) and corresponding simulated electron diffraction patterns from model (RHS).

the molecular symmetry plane (perpendicular to the longest molecular axis and passing through the double C=O bond) coinciding with the crystal mirror plane (perpendicular to the crystal *a*-axis). Moreover, the *a*-value is close to the length of the molecule in an extended conformation, implying that the longest molecular axis should lie along the crystal *a*-axis. In addition to this, we know from the strong SHG-effect that the dipole, which is perpendicular to the longest molecular axis, must be oriented such as to give rise to a large component in the *c*-direction perpendicular to the *ab*-plane.

4.1.4. DMABC crystal structure and orientation of molecules in the unit cell from simulation calculations

The simulations performed as described previously led to the crystal structure shown in Fig. 3 down the *a*

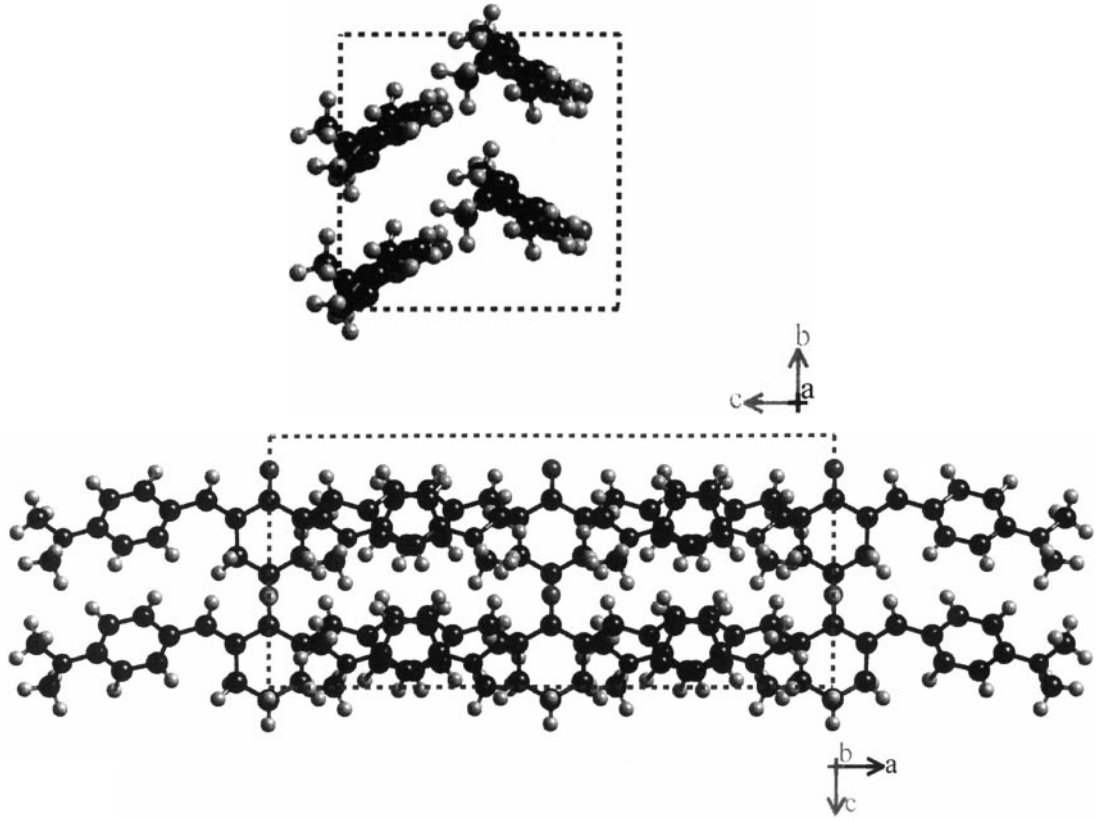

Figure 3 DMABC crystal structure obtained by simulation of electron diffraction patterns using packing energy calculations.

and *b* axes. The simulated diffraction patterns from this model for each zone are shown on the RHS of the corresponding experimental diffraction patterns in Fig. 2. The calculated packing energy per unit cell for the model structure is −643.5 kJ/mol.

4.1.5. Quantitative analysis of electron diffraction patterns

Quantitative analysis of the 100 kV electron diffraction data were registered on photographic film and subsequently quantified by a scanner as described previously [11, 43].

The temperature factor of the experimental data set was determined to be $B = 0.009$ nm^2 by a Wilson plot which gave a good linear relationship. This value is slightly low but still reasonable for organic crystals, especially when compared with the value of 0.025 nm^2 obtained for the theoretical data set from the model for the same intensity range. The average *R*-value from the original data set was 34%. The reasons for these relatively bad values were investigated and reported in detail elsewhere [11, 43]. Improvement in these *R*-values was obtained with MSLS [23], where dynamic effects, crystal tilt, absorption and crystal thickness are taken into consideration. The R_{MSLS}-factor is defined as:

$$R_{\mathrm{MSLS}} = \frac{\sum \left\{ I_{\mathrm{m}}^{\mathrm{obs}} - I_{\mathrm{m}}^{\mathrm{calc}} \right\}^2}{\sum \left\{ I_{\mathrm{m}}^{\mathrm{obs}} \right\}^2}$$

For 100 kV an *R*-value of 26.9% was obtained with a centre of Laue circle at (−5, 2) and a thickness of 24 nm [11]. The plots shown in Fig. 4 indicate how these minima behave as a function of (h, l) at 100 kV and also at 300 kV (minimum at 16%). Therefore, by taking account of dynamical effects the *R*-vaue at 100 kV decreases by 10% to 26% and at 300 kV the *R*-value is reduced by another 10%. The reasons for this improvement are very complex and have been treated elsewhere [43].

4.1.6. Structure solution using maximum entropy and likelihood

The data set from this sample comprised 133 crystallographically unique reflections. The maximum resolution of the data in favourable zones was 0.1 nm, but in practice, the effective resolution of the data was nearer 0.2 nm because many zones contained fewer reflections. The data were less than 30% complete. These features make the structure solution very difficult using traditional methods.

A typical centroid map is shown in Fig. 5 [11]. The projections down the a and b unit cell axis are shown. In all cases the effective resolution of 0.15–2.0 nm precludes seeing a structure at the atomic level. Rather, one sees an envelope with some atomic detail. It is possible to superimpose the simulated model structure on these maps. The crosses on the maps show the positions of the refined atomic co-ordinates. Most of the features in the maps are accounted for.

4.1.7. Quantum mechanical calculation of crystal properties

The structure analysis showed that the DMABC molecule lies in the molecular *xy*-plane forming an angle $\alpha = 27.74^\circ$ with the 2-fold screw *c*-axis of the crystal (*Z*-axis of the crystal frame) [11]. The line of

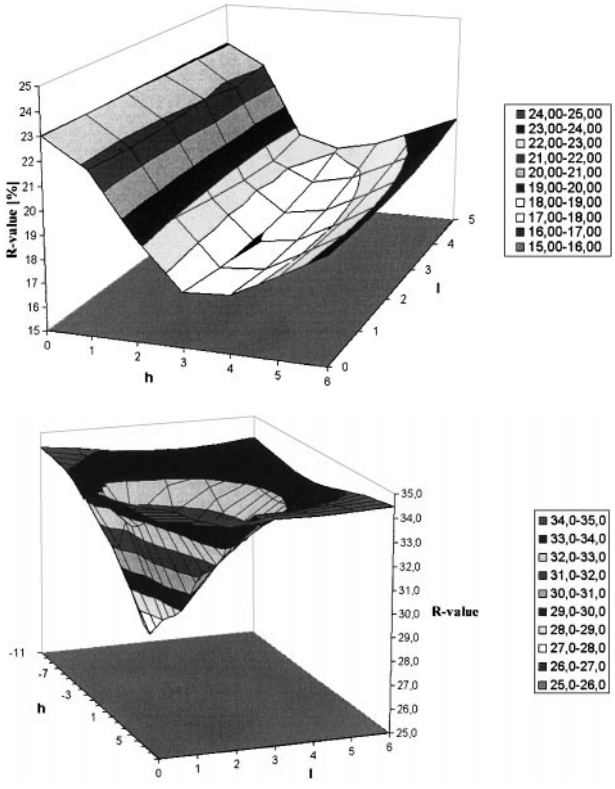

Figure 4 R-values for DMABC using 300 KV (top) and 100 KV (bottom) data.

intersection of the molecular xy-plane by the XY-plane of the crystal is parallel to the mirror XZ-plane of the crystal, which, according to the convention used by Zyss [44], indicates that the second angular parameter for groups $mm2$, $\Phi = 0$. The longest x-axis of the molecule in the cell is along the X-axis of the crystal frame.

The results of the MOPAC calculations of the molecular β-tensor components necessary for the calculations within the two-dimensional model are [19]

$$\beta_{yyy} = 0 \quad \beta_{yxx} = 7.5 \times 10^{-30} \text{ esu} \quad \beta_{xyy} = 0$$

This leads to the following results:

$$b_{ZZZ} = \beta_{yyy} \cos^3\alpha = 0$$

$$b_{ZYY} = \frac{-\beta xyy(\sin 2\Phi \sin 2\alpha)}{2} + \beta_{yxx} \sin^2\Phi \cos\alpha + \beta_{yyy} \cos^2\Phi \cos\alpha \sin^2\alpha = 0$$

$$b_{ZXX} = \frac{\beta_{xyy}(\sin 2\Phi \sin 2\alpha)}{2} + \beta_{yxx} \cos^2\Phi \cos\alpha + \beta_{yyy} \sin^2\Phi \cos\alpha \sin^2\alpha = 6.6 \times 10^{-30} \text{ esu}$$

The calculated d_{ZXX} coefficient is:

$$d_{ZXX} = \left(\frac{N}{V}\right) f_Z (f_X)^2 b_{ZXX} = 85.7 \times 10^{-9} \text{ esu} = 35.7 \text{ pm/V}$$

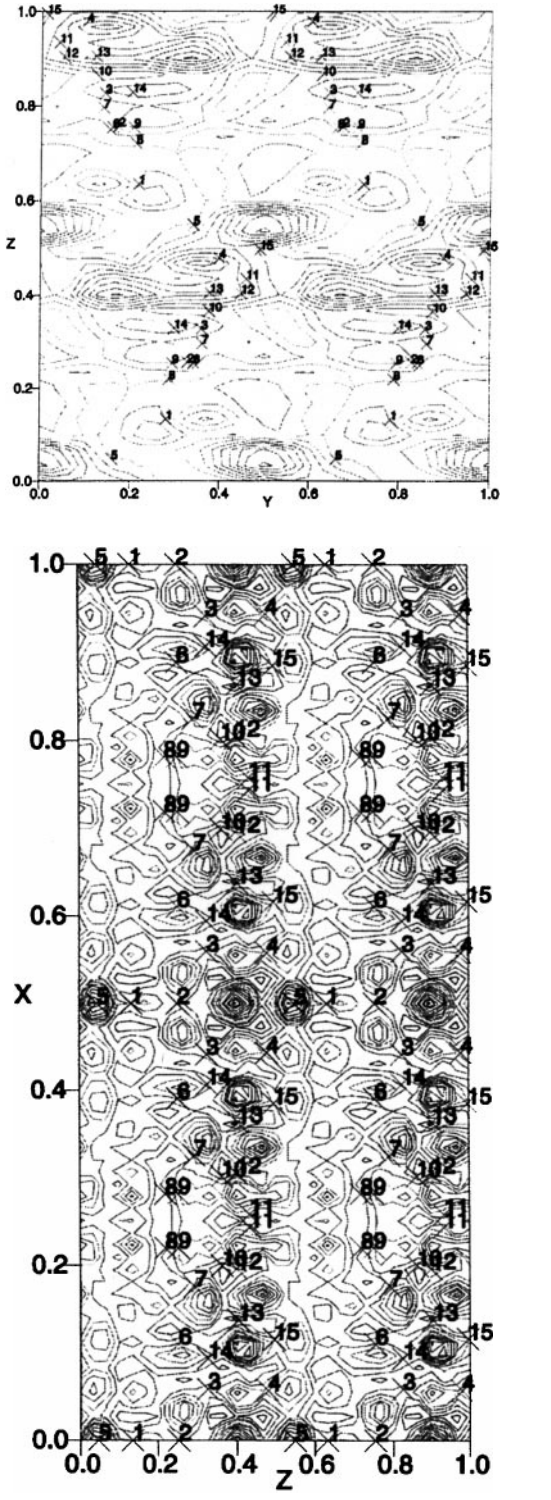

Figure 5 DMABC centroid maps from electron diffraction data obtained by maximum entropy calculations. Atom positions are marked by numbers.

In semi-empirical calculations the molecular α-tensor components (and therefore the local field factors)are frequently underestimated [11]. Those calculated by *ab initio* methods, on the other hand are too large [11]. For DMABC a value of 370 pm/V was calculated for d_{zxx}, which is three times larger than the experimental value. The *ab initio* calculated molecule and dipole direction are shown in Fig. 6.

These results show that the packing of DMABC molecules in the crystal is much more favorable with respect to the realization of NLO-properties than the

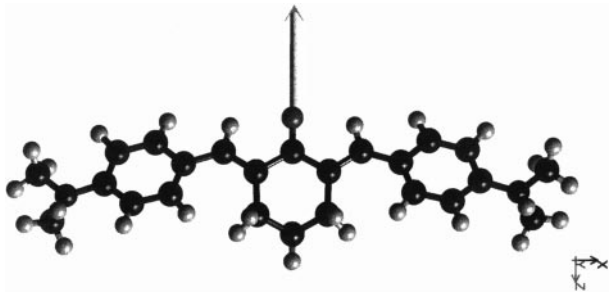

Figure 6 Gas phase conformation of DMABC molecule calculated by *ab initio* DFT methods showing direction of dipole.

crystal packing of the standard urea. While for the urea crystal $b_{XYZ} = 0.5\beta_{yxx}$, for the DMABC crystal structure $b_{ZXX} = 0.87\beta_{yxx}$. It should be noted that, since β_{yxx} enters the expression for b_{ZXX} with the coefficient $\cos^2 \Phi \cos \alpha$, the molecular non-linearity of a molecule of this type might even be completely transformed into the crystalline nonlinearity if a crystal structure with $\Phi = \alpha = 0$ is realised. In our opinion, this is a potentially very important advantage of the two-dimensional molecules such as DMABC over the one-dimensional systems, for which only 38% at maximum of molecular non-linearity may be transformed into crystalline nonlinearity [19, 11] It should be noted that the DMABC crystal may have both dipolar and octopolar contributions to the macroscopic second-order polarisability since it is an *mm*2-medium and the local symmetry of the molecules in the unit cell is close to C_{2v} [45].

The nature of this contribution may be interpreted within the three-state model (ground state, *g*, plus two excited electronic states, *a* and *b*), its magnitude being proportional to the product $\Delta\mu_{ga}\Delta\mu_{ab}\Delta\mu_{bg}$ ($\Delta\mu_{ij}$ is the transition dipole moment between the states i and j). The relationships between the magnitude of the octopolar contribution and the molecular β-tensor components for the specific cases of special symmetries have been considered in many publications by Zyss.

4.2. BHBC

4.2.1. Electron diffraction

Optical Measurements on BHBC using the method described previously [17] gave a rather low intensity of SHG green light. This result is an indication that the unit cell is non centrosymmetric. However, either the individual components of the hyperpolarisability tensor are very small or many components mutually cancel.

Two possible orthorhombic space groups were consistent with the observed extinction *s*, namely *Pnma* and $Pna2_1$ (International Tables of Crystallography). However, *Pnma* is a centrosymmetric space group, and $Pna2_1$ is non-centrosymmetric. Since the powder crystals show second harmonic generation (SHG), the only possible space group was $Pna2_1$ with cell parameters: $a = 1.170$ nm, $b = 3.489$ nm, $c = 0.764$ nm [10].

From these values of cell parameters it is obvious that the asymmetric unit of the unit cell contains two independent BHBC molecules in order to give a reasonable density. Moreover, the *b*-value is close to the double length of the molecule in an extended conformation. This suggests that the asymmetric unit is a linear dimer with an H-bond between terminal OH-groups of the two BHBC molecules. It is also clear that this H- bonded dimer itself cannot be centro-symmetric or nearly centro-symmetric, because then all of its molecular hyperpolarizability tensor components β_{ijk} would be zero. Then the crystal would not have an SHG-effect, regardless of the space group.

4.2.2. BHBC crystal structure and orientation of molecules in the unit cell from simulation calculations

The simulations give an atomic distribution shown in Fig. 7a and b [10]. The packing energy was calculated to be −1213 kJ/mol/unit cell. The asymmetric unit of the unit cell is a dimer of BHBC molecules H-bonded through terminal OH-groups, one of the molecules being H-donor and the other H-acceptor in the H-bond. The inertia axes of this H-bonded dimer are almost exactly parallel to the crystal axes (the longest axis of the dimer is parallel to the crystal *b*-axis). The crystal structure presents H-bonded layers of BHBC molecules without interlayer H-bonding. The H-bonding between neighboring asymmetric units within each layer is realized between the hydroxy-group of one molecule and carbonyl group of the other.

4.2.3. Quantitative analysis of electron diffraction patterns

The *R*-factor for the complete 100 kV data set was found to be 26%. This value is reasonable for an uncorrected electron diffraction data set and indicates that the data set is reliable.

The temperature factor of the experimental data set was determined to be $B = 0.0123$ nm^2 by a Wilson plot which gave a good linear relationship. This value is slightly low but still reasonable for organic crystals, especially when compared with the value of 0.025 nm^2 obtained for the theoretical data set from the model for the same intensity range. In our opinion this is due to the limited number of parameters available for this large unit cell containing 8 molecules. This value thus indicates that the data are reliable.

4.2.4. Structure solution using maximum entropy and likelihood

The data were normalised as described previously and, as before, only the molecular outline is visible (Fig. 8) To impose atomicity, model building was then used in which the molecular model was superimposed on the map, rotating the model as necessary around the bonds which had the necessary torsional freedom. This method is used routinely in protein crystallography, for example, but is much less common in the small molecule crystallographic environment.

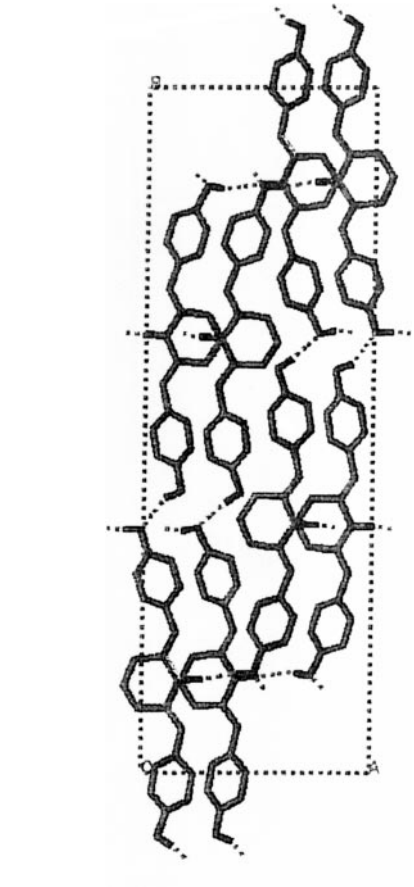

(a)

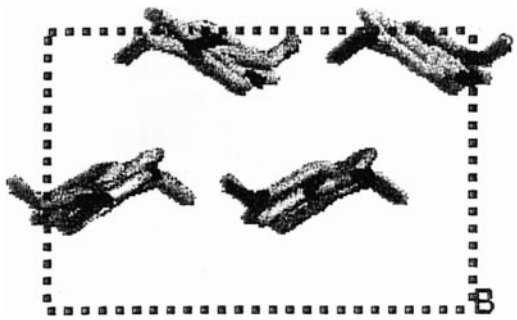

(b)

Figure 7 Calculated model of BHBC indicating hydrogen bonds . . . and showing [001] projection (a) and [010] projection (b).

4.2.5. Quantum mechanical calculations of the molecular polarisabilities and their relationships to macroscopic NLO-coefficients of the BHBC crystal

The molecular α-tensors calculated by both the PM-3 and 6-31G(+sp, +sd) *ab initio* methods for the asymmetric unit (H-bonded BHBC-dimer) of the crystal were reduced to the crystal frame to give the α_{IJ} components of the resultant α-tensor of the unit cell per molecule. The results are summarised in Table III of ref [10]. It is shown there that the PM-3 method underestimates linear polarisability tensor components, especially α_{ZZ}. *Ab initio* data presented in Table IV of the same paper show that frequency dependence influences considerably only the α_{YY}-value and the corresponding local-field factor, f_Y.

The largest component of the molecular β-tensor for the dimeric asymmetric unit is β_{xxx}, characterising the intramolecular charge transfer along the molecular longest x-axis of the asymmetric unit. Therefore this H-bonded BHBC dimer itself might be considered as a one-dimensional NLO-chromophore. However, the observed NLO-effect of the BHBC crystal powder cannot be due to β_{xxx} because the molecular x-axis is exactly perpendicular to the crystal 2_1-axis (c-axis), leading to cancellation of the one-dimensional contribution. Similarly, two-dimensional contributions due to β_{xyy} and β_{yxx} vanish upon taking into account the crystal symmetry because the molecular xy-plane is exactly perpendicular to the crystal 2_1-axis. Therefore, the BHBC crystal NLO-properties can only be related to two-dimensional charge transfer in yz- and xz-molecular planes parallel to the crystal c-axis, the only relevant non-zero β-component being β_{zxx}. For this reason, a two-dimensional model, as proposed by Zyss [2, 45] was used for this crystal structure. Taking then into account the permutation between the molecular x- and y-axes (the longest x-axis of the H-bonded BHBC dimer in the unit cell is parallel to the Y-axis of the crystal frame, while it would be along the X-axis of the crystal frame according to the axes convention used by Zyss [44, 45] $b_{ZYY} = \beta_{zxx} = 1.0 \times 10^{-30}$ esu, according to the PM-3 estimation.

Thus, the estimated d_{ZYY} coefficient is: PM-3:

$$d_{ZYY} = \left(\frac{N}{V}\right) f_Z (f_Y)^2 b_{ZYY}$$
$$= 8.8 \times 10^{-9} \text{ esu} = 3.67 \text{ pm/V}$$

ab initio (static local-field factors):

$$d_{ZYY} = \left(\frac{N}{V}\right) f_Z (f_Y)^2 b_{ZYY}$$
$$= 17.9 \times 10^{-9} \text{ esu} = 7.45 \text{ pm/V}$$

ab initio (frequency-dependent local-field factors):

$$d_{ZYY} = \left(\frac{N}{V}\right) f_Z(2\omega, \lambda = 532 \text{ nm}) f_Y^2$$
$$\times (\omega, \lambda = 1064 \text{ nm}) b_{ZYY} = 21.5 \times 10^{-9} \text{ esu}$$
$$= 8.97 \text{ pm/V}$$

These calculated values, based on our structure analysis, confirm the qualitative result that the optical susceptibility of BHBC is much lower than that of DMBC. The reason for this is that the large β_{xxx} components mutually cancel and only the smaller $\beta_{zxx} = b_{zyy}$ (Zyss notation) components add up and contribute to the macroscopic susceptibility.

With respect to the quantitative values, the BHBC results show the same tendency as those for DMABC, namely that the *ab initio* values are considerably higher than those obtained by semi-empirical calculations.

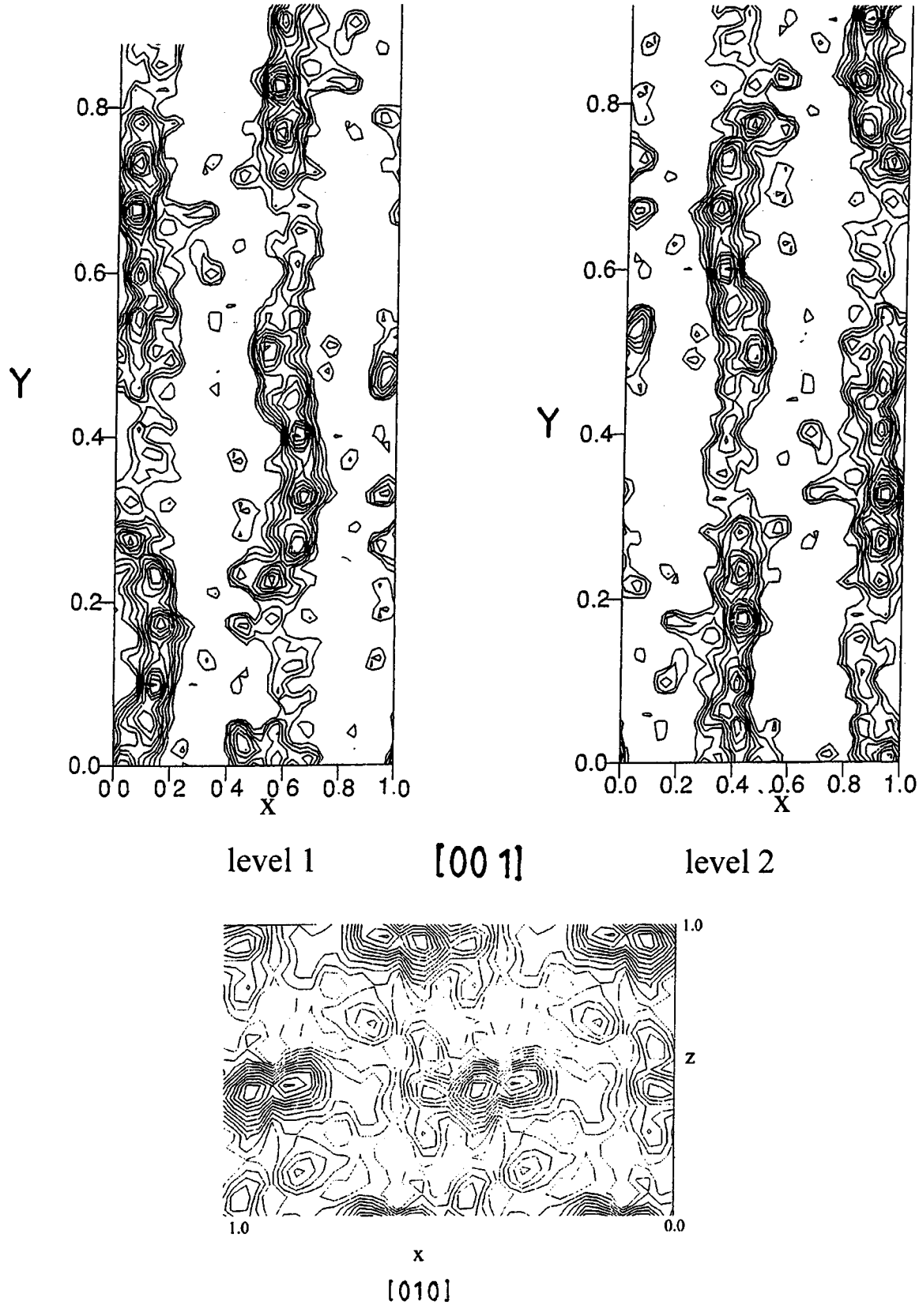

Figure 8 Centroid maps fromBHBC in the projections shown.

4.3. BMHBC

4.3.1. Gas-phase and crystal BMHBC molecular

The completely optimized *ab initio* gas-phase BMHBC conformation is shown in Fig. 9a [12]. The torsion angle of the phenyl rings is symmetric with respect to the central C=O double bond and is found to be ca. 20°.

4.3.2. Electron diffraction

The crystals did not give rise to a second order non-linear optical effect, although the individual molecules had a considerable second order transition. Thus, based on the extinctions and the physico-chemical properties, the centro-symmetric $P2_1/c$ space group was a definite possibility. Therefore these crystals

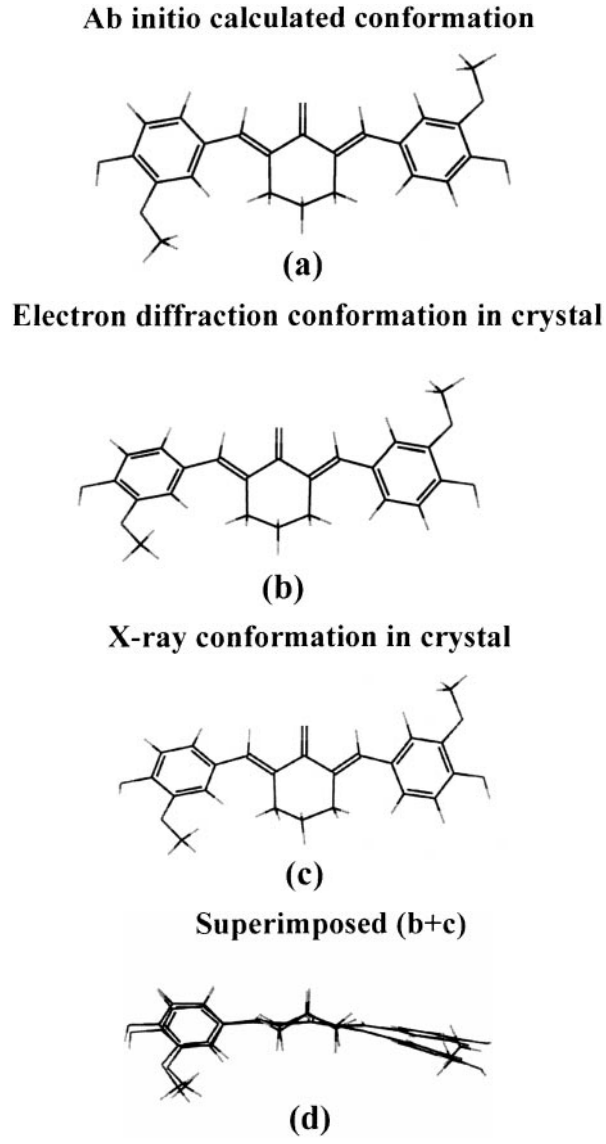

Figure 9 BMHBC conformation obtained by different methods.

cannot be used for SHG purposes. However, in view of the far-reaching consequences on the physical properties, it is important to understand the reasons for the difference with respect to DMABC and BHBC. Therefore the structure was refined.

4.3.3. Crystal packing and simulation of electron diffraction patterns

Different molecular conformations (sets of torsion angles), chosen manually around the initial *ab initio* gas-phase conformation, were used as starting models for the crystal packing energy minimization procedure. Among crystal structures thus obtained, the optimal structure corresponding to local minima of the packing energy was chosen. This crystal structure is shown in Fig. 10. Its packing energy value is −410 kJ/mol per cell. This value is not as low as those which we had obtained for BHBC and DMABC, but in this case it was impossible to reduce the packing energy further.

It should be noted that the molecular conformation in this crystal is non-symmetrical with respect to the central C=O bond (Fig. 9b). Namely, torsion angles between the phenyl rings and the C=C double bonds,

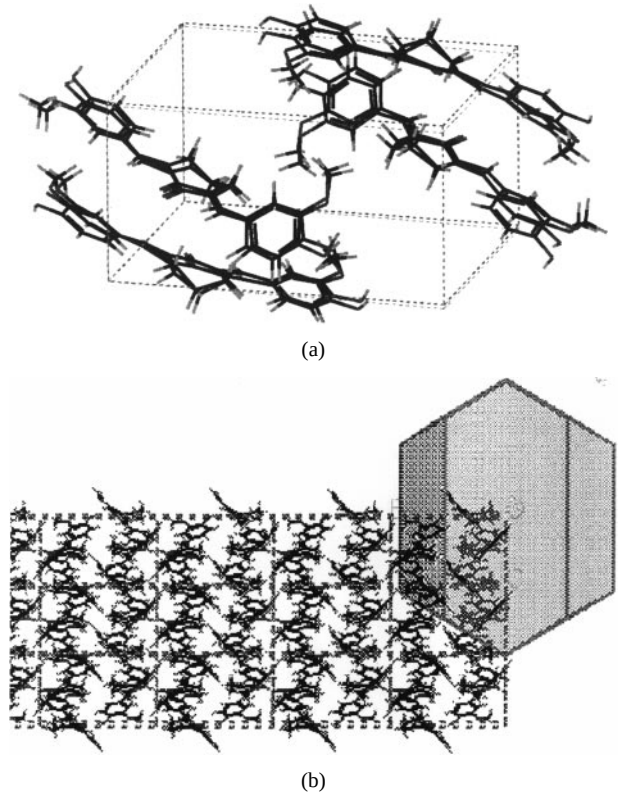

Figure 10 BMHBC molecule in unit cell showing effect of different conformations (a) and relationship between unit cell and crystal (b).

are −42° on one side of the molecule and 3.7° on the other. Details are reported elsewhere [12].

4.3.4. Quantifying the electron diffraction data

The quantitative values were compared with the kinematical values obtained from the initial electron diffraction model and the *R*-factor was found to be very high at 49%. It is obvious that the suggested structure (Fig. 10) still requires refinement to reduce this high *R*-factor value. However, the packing energy minimization procedure was unable to remove this discrepancy.

4.3.5. Maximum entropy structure determination

The 261 unique electron diffraction intensities were normalized to give a unitary structure factor and the [010] projection is shown in Fig. 11b. It is clearly seen that the four molecules are arranged at an angle with respect to the longest crystal axis in the unit cell. This confirms the model obtained from packing energy calculations in Fig. 11a. From these potential maps it is possible to recognise the arrangements and directions of the molecules in the unit cell but not the individual atoms.

In ref. [12] different projections from the simulated electron diffraction model are shown and compared with the maximum entropy maps. Most of the atomic positions in the potential maps correspond to high potential field positions while some of them appear in between high potential regions. Clearly the correct structure has not been found.

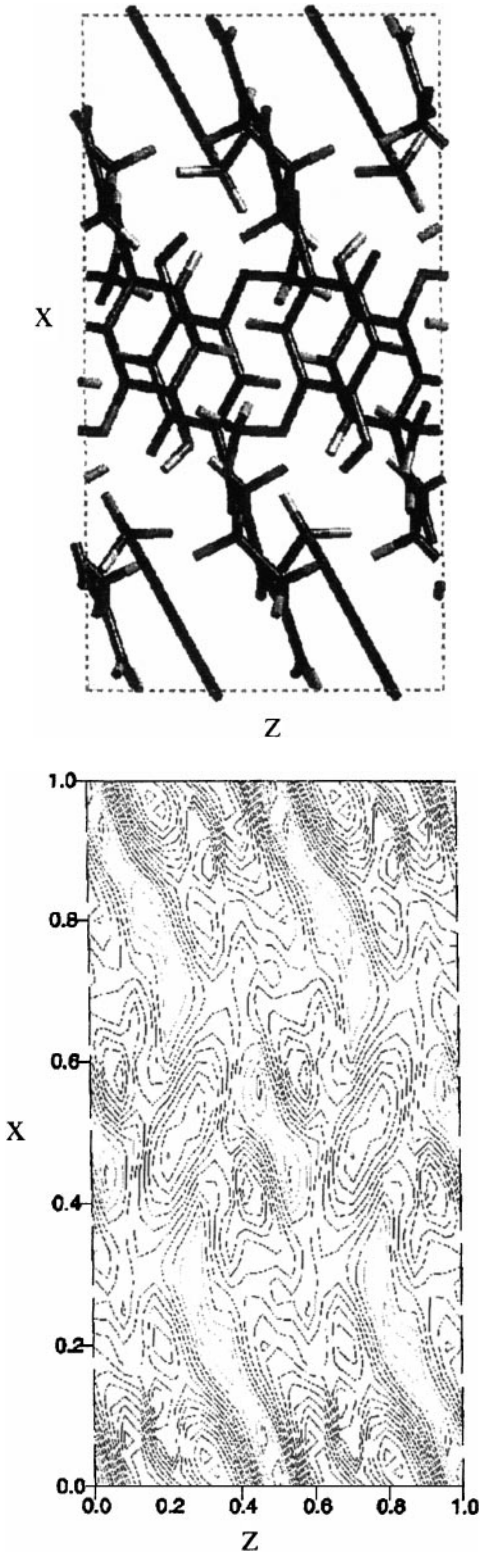

Figure 11 Model and centroid map of BMHBC.

4.3.6. Full X-ray analysis and refinement

All the experiments and calculations on BMHBC indicated some of the atomic positions found by simulation of electron diffraction patterns were incorrect. Therefore single crystals were grown and a full X-ray analysis undertaken.

For X-ray analysis large single crystals are required and these could not be obtained by the procedure described for electron diffraction. Instead, the BMHBC was dissolved as before but crystallized for two months at room temperature. The experimental details of the X-ray structure analysis are summarized elsewhere [12]. Since polymorphism frequently occurs in organic crystals, there is always a risk that a different crystal structure is produced. This becomes obvious when discrepancies occur.

The structure of these crystals was solved by direct methods [12] using SIR92 [46] and refined by full-matrix least square analysis using SHELX97 [47]. The data were reduced. Lorentz and polarization corrections were applied using a local data reduction program. Non-H atoms were refined anisotropically, H atoms were placed at geometrically calculated positions and refined isotropically with riding motion. It was found that calculated electron diffraction patterns from this structure corresponded more closely to the experimental electron diffraction data. In order to illustrate the reason for the discrepancy, Fig. 9d shows an overlap of the molecular conformations in the crystal from packing energy plus simulation calculations and from X-ray single crystal analysis. In Fig. 10 the two structures are shown in a manner which highlights both the similarities at the centre of the molecule and the differences at the end groups. At the same time it also illustrates very clearly the limits of packing energy calculations for molecules having too many degrees of torsional freedom. While the packing energy of the correct structure was, as expected, lower than that of the model obtained by simulation, we were unable to find the global minimum of the unknown structure. However it was comforting to find that all our results had indicated that the correct structure had not been found.

4.3.7. Comparison of gas-phase and crystal BMHBC conformations

The reason for our inability to obtain a good model for the BMHBC crystal from packing energy calculations was the difficulty in ascertaining the correct rotation of the torsion angle of the phenyl rings due to the crystal field [12]. This is in marked contrast to the other molecules in this series [10, 11]

The completely optimized gas phase conformation of BMHBC is symmetric with respect to the central C=O double bond: the torsion angles between phenyl rings and C=C double bonds are about 20°. However, the molecular conformation, found both in packing energy calculations and in the X-ray single crystal structural analysis, is non-symmetric: in the conformation from X-ray analysis one of the two torsion angles is ca. 30° and the other is almost zero. It should be noted that values of these torsion angles are determined by a compromise between the π-electron conjugation (favouring flat conformation) and steric repulsion between aromatic and olefinic protons (favouring strongly torsioned conformation). One possible solution may be symmetrical torsion on both sides of the molecule, and it is the situation that is realized in the gas-phase. The other possible compromise is to make the torsion more profound on one side of the molecule and to reduce it (almost up to zero) on the other side. This is the situation realized in the crystal BMHBC structure. Such

a non-symmetric conformation did not correspond to a gas-phase potential energy surface local minimum. However, the potential energy surface is rather flat with respect to these torsions: changing the torsion angles by ca. 20° leads to only 4.2 kJ/mol change in the total energy [12]. It is reasonable to assume that the non-symmetric BMHBC conformation in the crystal state is induced by the crystal field effect, especially by the intermolecular H-bonding contribution into the total energy.

4.4. Polymer

4.4.1. Simulation of electron diffraction patterns based on structure of model substances

In general crystal structure analysis and refinement of polymer crystals is impossible because the number of reflections is too small. However, if the monomeric unit is well characterised as in this case, it may be possible to simulate the diffraction patterns using packing energy calculations. In this case it is essential to supplement the available information with an x-ray powder pattern and to simulate this as well as the rather sparse electron diffraction patterns. This procedure was used for BMHBCpol. and a tentative model proposed [48].

Using CERIUS 2.0 simulations, the NLO-active polymer BMHBCpol. was found to crystallize in an orthogonal unit cell with monoclinic symmetry (unique a-axis): Space group $P2_111$; $Z = 2$; $d = 1050$ kg/m^3; $a = 0.74$ nm; $b = 1.13$ nm; $c = 1.96$ nm; $\alpha = 90^\circ$.

The projection of the proposed polymer crystal structure along the monoclinic a-axis is shown in Fig. 12 . In order to solve this structure, the $P2_1/c$ crystal structure of the low molecular weight analog BMHBC [12] was used as an initial model. For the polymer model, the cycles of cell parameter refinement and crystal packing energy minimization were performed until a reasonable agreement between the simulated and experimental X-ray powder diffraction and reasonable packing energy (ca. −293 kJ/mol/cell) was achieved. This procedure finally resulted in a non centro- symmetric structure [48]. The molecule exhibits a zig-zag conformation and segregation of the aliphatic and aromatic parts, but the packing energy indicates that further refinement is required.

5. Conclusion

5.1. Comparison of the structures found for this series of bis-benzylidene cyclohexanones

The 2,6-bis-benzylidene-cycloalkanones were extensively studied by us [10–12] and other groups [49]. Some of the compounds of this class, such as 2,6-bis-(4-dimethylamino-benzylidene)-cyclohexanone (DMABC) [11, 19, 49, 50] and 2,6-bis-(4-hydroxy-benzylidene)-cyclohexanone (BHBC) [10, 50] display a macroscopic nonlinear optical (NLO) second harmonic generation (SHG) effect in the crystal state. In the DMABC crystal structure, which has the largest NLO effect, ca. 50 times that of urea [51] the DMABC molecules occupy special positions in the $Cmc2_1$ space group with the crystal mirror plane passing through the C=O double bond. Thus, the DMABC crystal state conformation is completely symmetric with respect to the C=O double bond. The BHBC crystal state conformation is also nearly symmetrical, although it is not restricted by its space group ($Pna2_1$) symmetry conditions.

Unfortunately the largest components of the hyperpolarisability tensor of BHBC cancel and only minor components contribute to the macroscopically observed optical susceptibility.

Finally, BMHBC is the molecule in this series which has the lowest conformational symmetry and was therefore expected to produce a good optical response. In fact, however, it is the only one in this group which crystallises in a centro-symmetric space group.

It appears that H-bond network formation is the main structure-determining factor for both the BHBC and BMHBC crystal structures. In many cases, intermolecular H-bonding in the crystal state leads to a non-centrosymmetric arrangement of molecules and it is explored in SHG-active crystal engineering strategies [52, 53]. Unfortunately, this is not the case for the BMHBC crystal structure. In fact, the H-bonding patterns for the two structures are rather similar [11, 12]. In both structures, there are linear chains of molecules H-bonded through their terminal OH-groups. In the BHBC crystal structure these linear chains are along the [0 1 0]-direction, while in the BMHBC case they are along the [1 0 $\bar{1}$]-direction. The interchain H-bonds in both cases are those between hydroxyl protons in a given chain and carbonyl oxygen atoms in the neighboring one.

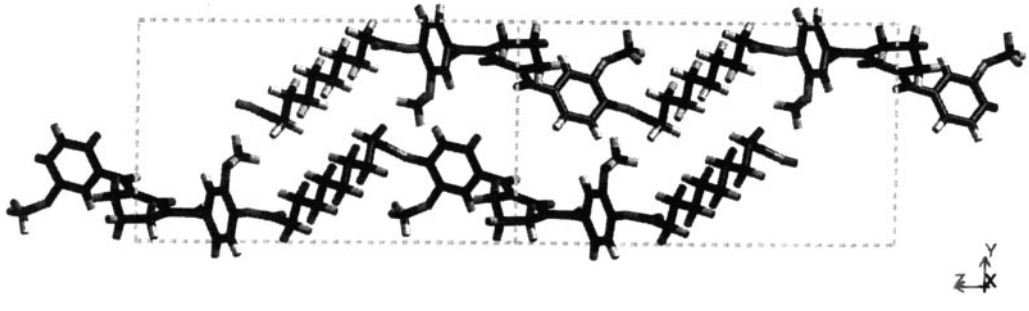

Figure 12 Simulated structure of BMHBC polymer.

According to a recent suggestion [54], for 2,6-bis-benzylidene-cycloalkanones, the structure-determining factor mainly responsible for non-centrosymmetric packing are intermolecular H-bonds of the C–H···O type between methylene hydrogen atoms in the cycloalkanone ring of one molecule and oxygen atoms of the surrounding molecules. Such H-bonds mostly form with carbonyl oxygen atoms as H-acceptors. In this case, the C–H···O and H···O=C bond angles are in the range of 120–180° [55, 56] and about 120° [56, 57], respectively. No contacts of such type are observed in the BMHBC centrosymmetric crystal structure [12]. In the case of the BHBC non- centrosymmetric crystal, such contacts do exist, but they are between methylene hydrogen atoms of a given molecule and hydroxyl oxygen (rather than carbonyl oxygen) atoms of the neighboring molecule [10].

5.2. Methods

The limitations of the simulation approach are related to the difficulty of finding a global rather than a local minimum for the molecular conformation and the necessity of determining the effect of the crystal field on this conformation. Packing energy considerations [58–60] involve force field calculations which cannot be expected to perform well for all types of molecules and crystal structures. Therefore, one cannot expect the crystal packer to automatically find the global minimum of the crystal packing energy multidimensional surface with the accuracy in atomic positions necessary to get a good crystallographic *R*-factor. Adjustments based on chemical knowledge need to be made by the operator. Frequently information about chemically similar moecules is essential. This can often be found in the Cambridge data base. In most cases it is necessary to modify the molecular torsion angles within the molecule manually to try to get better agreement between the experimental and calculated electron diffraction patterns. However, for molecules with many torsional degrees of freedom like BMHBC, this manual procedure cannot cover all possible conformations. Due to the many factors affecting the global minimum of this multidimensional energy surface, a good series of experimental electron diffraction patterns is essential, because a comparison between experimental intensity distributions and those calculated from the model immediately indicates whether the latter is reasonable.

In those cases where the optimized gas-phase conformation is not significantly affected by the crystal field, we have shown in the past [10–13, 18–21] that this refinement is possible.

A serious limitation of the Crystal Packer is that it cannot optimise subrotations within cyclic molecular fragments. However, such subrotations, determining the conformation of, e.g., cyclohexanone fragments of BMHBC and other 2,6-bis-benzylidene-cyclohexanones, are important for reducing the *R*-factor but, unfortunately, can only be guessed.

We have shown here that structure determination and refinement is possible from an electron diffraction data set by combining the simulation calculations with the Maximum Entropy approach. In addition, it has been shown that a dramatic improvement in *R*-factor can be obtained at 300 kV and with on-line CCD data acquisition. Our results therefore indicate that these methods to solve and refine the structure of small organic molecules will be used routinely in the coming years. Then specific physico-chemical properties of materials can be induced by directed synthesis on condition that the associated parameters are understood at a molecular level.

Acknowledgements

This paper summarises work which has been performed in my laboratory during the past 5 years, so that many research students and post docs have made invaluable contributions. These are A. Yakimanski, H. Kothe, U. Kolb, Gao Li, R. C. Yu. In addition, there has been a very fruitful collaboration with the groups of C. Gilmore, H. Zandbergen, R. Wortmann and A. Tenkovtsev. However, my interest in organic crystals was initially aroused by the work of Andrew Keller. Financial support over many years by the Deutsche Forschungsgemeinschaft is gratefully acknowledged.

References

1. G. R. DESIRAJU, "Materials Science Monographs 54: Crystal Engineering" (Elsevier, 1989).
2. D. S. CHEMLA and J. ZYSS, in "Non-linear and Optical Properties of Organic Molecules and Crystals," ed. (Academic Press, 1987).
3. D. DORSET, "Structural Electron Crystallography" (Plenum Press, 1995).
4. G. BRICOGNE, *Acta. Cryst. A* **40** (1984) 410.
5. *Idem*., "Max. Entropy in Action," edited by B. Buck and V. A. Macauley (1991).
6. C. GILMORE, G. BRICOGNE and G. BANNISTER, *Acta. Cryst. A* **46** (1990) 297.
7. C. GILMORE, K. SHANKLAND and G. BRICOGNE, *Proc. Roy. Soc. (Lond)* **442** (1993) 97.
8. I. G. VOIGT-MARTIN, D. H. YAN, A. YAKIMANSKI, D. SCHOLLMEYER, C. J. GILMORE and G. BRICOGNE, *Acta Crystallogr. A* **51** (1995) 849.
9. I. G. VOIGT-MARTIN, D. H. YAN, C. J. GILMORE, K. SHANKLAND and G. BRICOGNE, *Ultramicroscopy* **56** (1994) 271.
10. I. G. VOIGT-MARTIN, GAO LI, U. KOLB, H. KOTHE, A. V. YAKIMANSKI, A. V. TENKOVTSEV and C. GILMORE, *Phys. Rev. B.* **59** (1999) 6722.
11. I. G. VOIGT-MARTIN, H. KOTHE, A. V. YAKIMANSKI, A. V. TENKOVTSEV, H. ZANDBERGEN, J. JANSEN and C. GILMORE, *Ultramicroscopy* **83** (2000) 33.
12. R. YU, A. YAKIMANSKI, H. KOTHE, I. G. VOIGT-MARTIN, C. GILMORE, J. JANSEN and H. ZANDBERGEN, *Acta. Cryst. A*, in print (2000).
13. I. G. VOIGT-MARTIN, Z. X. ZHANG, D. H. YAN, A. YAKIMANSKI, R. MATSCHINER, P. KRÄMER, C. GLANIA, D. SCHOLLMEYER, R. WORTMANN and N. DETZER, *Colloid Polym. Sci.* **275** (1997) 18.
14. J. C. H. SPENCE and J. M. ZUO, "Electron Microdiffraction" (Plenum Press, 1992).
15. J. J. P. STEWART, "MOPAC 6.0, A General Purpose Molecular Orbital Package" (QCPE, 1990).
16. W. G. RICHARDS and D. L. COOPER, "Ab initio Molecular Orbital Calculations for Chemists," 2nd ed. (Oxford University Press, 1983).
17. M. LOOS-WILDENAUER, S. KUNZ, I. G. VOIGT-MARTIN, A. YAKIMANSKI, E. WISCHERHOFF, R. ZENTEL, C. TSCHIERSKE and M. MÜLLER, *Advanced Materials* **7** (1995) 170.
18. R. YU, A. V. YAKIMANSKI, I. G. VOIGT-MARTIN, A. FETTEN, D. SCHOLLMEYER and H. MEIER, *J. Chem. Soc., Perkin Trans*. **9** (1999) 1881.

19. A. YAKIMANSKI, I. G. VOIGT-MARTIN, U. KOLB, G. N. MATVEEVA and Z. X. ZHANG, *Acta Cryst A* **53** (1997) 603.
20. I. G. VOIGT-MARTIN, D. H. YAN, R. WORTMANN and K. ELICH, *Ultramicroscopy* **57** (1995) 29.
21. I. G. VOIGT-MARTIN, Z. X. ZHANG, U. KOLB and C. GILMORE, *ibid*. **68** (1997) 43.
22. U. KOLB and H. KOTHE, "NATO ASI Series: Electron Crystallography," Vol. 347 (Kluwer, Dordrecht, 1997) p. 383.
23. J. JANSEN, D. TANG, H. W. ZANDBERGEN and H. SCHENK, *Acta Crystallogr. A* **54** (1998) 91.
24. A. WILLETS, J. E. RICE, D. M. BURLAND and D. P. SHELTON, *J. Chem. Phys*. **97** (1992) 4590.
25. K. CLAYS and A. PARSOONS, *Phys. Rev. Letters* **66** (1992) 3258.
26. B. F. LEVINE and C. G. BETHEA, *J. Chem. Phys.* **63** (1975) 2666.
27. A. GAVEZOTTI, *J. Am. C hem. Soc*. **113** (1991) 4622.
28. G. FILLIPINI and A. GAVEZOTTI, *Acta. Cryst. B* **49** (1993) 868.
29. H. KURTZ and J. STEWART, *J. Comput. Chemistry* **11** (1990) 82.
30. R. W. TERHUNE, P. D. MAKER and C. M. SAVAGE, *Phys. Rev. Letters* **66** (1965) 681.
31. J. J. WOLFF, D. LÄNGLE, D. HILLENBRAND, R. WORTMANN, R. MATSCHINER, C. GLANIA and P. KRÄMER, *Adv. Materials*, in press.
32. K. CLAYS, A. PARSOONS and L. DEMAEYER, *Adv. Chem. Phys.* **85** (1994) 455.
33. R. G. PARR and W. YANG, "Density-Functional Theory of Atoms and Molecules" (Oxford Univ. Press, Oxford, 1989).
34. R. AHLRICHS, M. BÄR, M. HÄSER, H. HORN and C. KÖLMEL, *Chem. Phys. Lett*. **162** (1989) 165.
35. M. A. SPACKMAN, *J. Phys. Chem*. **93** (1989) 7594.
36. J. COWLEY, "Diffraction Physics" (Elsevier Publishers, 1986).
37. I. G. VOIGT-MARTIN, M. SCHUMACHER and R. GARBELLA, *Macromolecules* **25** (1992) 961.
38. X. ZOU, Y. ZUKHAREV and S. HOVMÖLLER, *Ultramicroscopy* **49** (1993) 147.
39. X. ZOU, in "NATO ASI Series: Electron Crystallography," Vol. 347, edited by D. Dorset, S. Hovmöller and X. Zou (Kluwer, Dordrecht, 1997) 383.
40. G. M. SHELDRICK, SHELXL93, Program for Crystal Structure Refinement, University of Göttingen, Germany, 1993.
41. C. J. GILMORE, W. DONG and G. BRICOGNE, *Acta Crystallogr. A* **54** (1998) 70.
42. C. J. GILMORE and G. BRICOGNE, *Methods in Enzymology* **277** (1997) 65.
43. H. KOTHE, Dissertation University of Mainz, 1998.
44. J. ZYSS and J. L. OUDAR, *Phys. Rev. A* **26** (1982) 2028.
45. J. ZYSS and I. LEDOUX, *Chem. Rev*. **94** (1994) 77.
46. A. ALTOMARE, G. CASCARANO, C. GIACOVAZZO, A. GUAGLIARDI, M. C. BURLA, G. POLIDORI and M. CAMALLI, *J. Appl. Cryst*. **27** (1994) 435.
47. G. M. SHELDRICK, SHELXL97, Program for Crystal Structure Refinement, University of Göttingen, Germany, 1997.
48. I. G. VOIGT-MARTIN, U. KOLB, H. KOTHE, A. YAKIMANSKI, R. C. YU and A. V. TENKOVTSEV, in Polymer Symposia, to be published.
49. J. KAWAMATA, K. INOUE and T. INABE, *Appl. Phys. Lett*. **66** (1995) 3102.
50. N. V. AGRINSKAYA, V. A. LUKOSHKIN, A. V. TENKOVTSEV and A. V. YAKIMANSKY, *Solid State Physics (in Russian)*. **39**(9) (1997) 183.
51. J. KAWAMATA, K. INOUE and T. INABE, *Mol. Cryst. Liq. Cryst*. **278** (1996) 117.
52. J. ZYSS, F. NICOUD and M. COQUILLAY, *J. Chem. Phys.* **81** (1984) 4160.
53. M. C. ETTER and G. M. FRANKENBACH, *Chem. Mater*. **1** (1989) 10.
54. J. KAWAMATA, K. INOUE and T. INABE, *Bull. Chem. Soc. Jap*. **71** (1998) 2777.
55. G. R. DESIRAJU, *Acc. Chem. Res*. **24** (1991) 290.
56. *Idem*., *ibid*. **29** (1996) 441.
57. A. BONDI, *J. Phys. Chem.* **68** (1964) 441.
58. A. GAVEZOTTI and G. FILLIPINI, *J. Am. Chem. Soc.* **118** (1996) 7153.
59. A. J. PERTSIN, A. KITAIGORODSKY, "The Atom-Atom Potential Method" (Springer-Verlag, Berlin, 1987).
60. A. GAVEZOTTI and G. FILIPPINI, *J. Amer. Chem. Soc.* **117** (1995) 12299.
61. I. G. VOIGT-MARTIN and U. KOLB, "Erice NATO Course on Electron Crystallography ASI" Series (1997).
62. J. M. COWLEY and A. F. MOODIE, *Acta Crystallogr*. **10** (1957) 609.

Received 17 January
and accepted 28 February 2000